Plant Stress 19 (2026) 101120

Contents lists available at ScienceDirect

Plant Stress

journal homepage: www.sciencedirect.com/journal/plant-stress

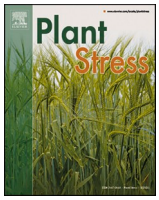

Multimodal signatures of stress: Revealing variations in blackleg expression across seed potato cultivars with UAV remote sensing

Magdalena Smigaj [a,d,*], Andries van der Meer [b], Jan van der Wolf [c], Lammert Kooistra [a]

[a] Laboratory of Geo-Information Science and Remote Sensing, Wageningen University & Research, the Netherlands
[b] Field Crops, Wageningen University & Research, Lelystad, the Netherlands
[c] Biointeractions & Plant Health, Wageningen University & Research, the Netherlands
[d] Scottish Environment Protection Agency, Stirling, United Kingdom

ARTICLE INFO

Keywords:
UAV remote sensing
Hyperspectral
Thermal
LIDAR
Disease detection
Plant stress
Agriculture

ABSTRACT

Remote sensing technologies offer a promising approach for detection of plant diseases, enabling timely interventions to prevent the spread and minimise financial losses. However, a major gap exists in understanding how cultivar and growth stage variations might influence the stress responses captured by different modalities, and subsequently affect disease detection capabilities. This study aimed to bridge this gap by exploring the variation in plant-level responses to blackleg onset (caused by *Dickeya* and *Pectobacterium* species) in six cultivars with varying susceptibility levels through investigation of metrics extracted from UAV hyperspectral, LiDAR, thermal data.

Whilst we found clear responses to infection in all modalities, substantial cultivar-based variations were present due to different levels of symptom expression. Hyperspectral data emerged as the most crucial for blackleg detection, with specific feature importance varying over the season. Early-season responses were most strongly reflected in PRI, while later in the season, PSRI became more informative. Thermal and structural metrics, while showing promise, exhibited varying sensitivity to infection across cultivars and growth stages, with significant variability observed even among healthy plants of different cultivars.

Combining modalities in SVM detection models offered small improvement in disease detection capabilities, though the use of hyperspectral and LiDAR data together yielded the most consistent performance across the investigated dates (balanced accuracy of 90–94 %). Still, models' performance was substantially affected by cultivar variations. These findings highlight the critical need to account for cultivar-specific responses and the dynamic nature of disease symptom expression when developing remote sensing-based disease detection models for arable crops.

1. Introduction

Plant diseases are becoming ever more destructive due to climate change, already causing up to 40 % losses in global production (IPPC Secretariat, 2021). At the same time intensive agricultural practices have caused substantial ecosystem degradation (Kopittke et al., 2019; Sánchez-Bayo and Wyckhuys, 2019), necessitating a shift towards more sustainable methods to reduce the pressure and mitigate the ongoing biodiversity loss. This urgent need is being increasingly recognised and implemented in national and international strategic plans. For example, in the EU this commitment is reflected in a number of initiatives like the European Green Deal, the Farm to Fork Strategy, and the Integrated Pest Management directive (Commission, 2020; Cuadros-Casanova et al., 2023; European Commission, 2019). These aim to promote practices favouring biodiversity within the agricultural landscape, sustainable food production methods, and reduced chemical reliance, which includes the dependence on fertilisers and pesticides.

Meeting these sustainability goals whilst ensuring optimal agricultural production requires development of effective ways for monitoring crop status to enable targeted interventions. This is crucial for curbing outbreaks, minimising yield losses and improving crop quality. In particular, prompt and accurate identification of biotic stress agents is key since different diseases may require different interventions, ranging from complete removal of affected plants to the application of

* Corresponding author.
E-mail address: magdalena.smigaj@sepa.org.uk (M. Smigaj).

https://doi.org/10.1016/j.stress.2025.101120
Received 30 January 2025; Received in revised form 28 August 2025; Accepted 2 November 2025
Available online 3 November 2025

pesticides. However, disease identification through the traditionally employed visual assessment of stress symptoms on the plants is labour-intensive and requires a high level of expertise. Remote sensing approaches are often suggested as more efficient alternatives. Their potential for precision agriculture has long been demonstrated (Mulla, 2013; Weiss et al., 2020) and so has their capability for capturing physiological responses to stress onset (Berger et al., 2022).

The different modalities of available sensors offer glimpses into different physiological responses of affected plants. Spectroscopy is primarily sensitive to changes in leaf biochemical properties, thermography can provide information on alterations in transpiration, LiDAR can capture plant structural changes (e.g. defoliation), whilst fluorescence imaging can capture variations in photosynthesis (Berger et al., 2022). Although the focus for a long time remained on the analysis of spectral responses, development of miniature sensors that can be mounted on Uncrewed Aerial Vehicles (UAVs) opened the possibility for concurrent exploration of these modalities. Their combination allows obtaining a more comprehensive picture of physiological responses, which can potentially help improve remote identification of ailing plants and allow matching these responses to specific stress agents.

Although multimodal approaches are being increasingly advocated for (Berger et al., 2022), UAV-borne and airborne studies on crop disease detection typically focus on the use of multispectral/hyperspectral data. Promising investigations into sensor synergies in disease identification context have largely been restricted to laboratory and proximal set-ups (Berger et al., 2022). The few existing UAV-borne/airborne investigations similarly highlighted the value of multimodal data for capturing different disease symptoms in non-woody crops (Franceschini et al., 2024; Maimaitijiang et al., 2020; Zhang et al., 2019), orchards (Poblete et al., 2023; Zarco-Tejada et al., 2018, 2021) and forests (Hornero et al., 2024; Smigaj et al., 2019a, 2019b; Yu et al., 2021; Zhang et al., 2023). However, previous multimodal studies, especially those utilising UAVs, were often restricted to a single stress agent, time point, and/or plant cultivar. This inevitably presents a simplified version of reality, ignoring the interdependence between cultivar-specific plant traits, differing resistance levels, plant growth stage, and resultant remote sensing metrics that are used as inputs for detection models, likely hindering transferability of the developed approaches to other cultivars, regions and growing seasons.

The physiological responses following disease onset are particularly complex and variable in nature, as they involve a continuous interplay between plant's resistance that depends on the utilised cultivar, the specific pathogen strain, and the prevailing environmental conditions that can affect plant's susceptibility to infection (Eastburn et al., 2011; Singh et al., 2023). Furthermore, disease symptoms can evolve over time, with the plant exhibiting a range of responses depending on the stage of infection. This dynamic differs from the more singular stress events typical of many abiotic factors. Understanding how these variations affect remote sensing metrics used in disease detection algorithms and how these metrics link to actual physiological responses is crucial for developing more robust and generalisable disease detection models that can be applied more widely. Yet, such investigations are largely missing outside of controlled indoor environments, partially due to the logistical challenges associated with establishing large-scale and diverse field trials.

This study aims to address this knowledge gap by exploring the impact of varying cultivars and plant growth stages on the remote sensing signatures of seed potato plants subjected to blackleg disease. To achieve this, we utilised six seed potato cultivars with varying susceptibility levels and employed three different sensor modalities (hyperspectral, LiDAR and thermal) to assess their potential for identification of diseased plants. Based on this analysis, we will provide recommendations on the development of multimodal remote sensing strategies for disease monitoring in arable crops.

2. Methodology

2.1. Blackleg causal agents and characteristics

Blackleg is an economically important disease caused by species within the genera *Dickeya* and *Pectobacterium* that affects potato cropping worldwide. In the Netherlands the predominant causal agent has undergone a temporal shift. Prior to 2000, *D. dianthicola, P. atrosepticum* and *P. parmentieri* were the most frequently isolated species. *D. solani* then emerged as the dominant causing strain between 2000 and 2010. Presently, specific haplotypes of *P. brasiliense* are typically associated with blackleg outbreaks.

The most dominant source of infection is the (latently-infected) seed tuber, which spreads the bacteria to the soil and neighbouring plants as the disease progresses. Inadvertent transmission can also occur during cutting and planting operations when contaminated tools come into contact with healthy tubers. The most characteristic disease symptom is a black soft rot, appearing at the stem base (see Fig. 1). The disease often starts with a darkening of the top leaves, followed by wilting, chlorosis and desiccation of leaves. Though, its virulence can vary substantially both across the species and individual strains. Aerial stem rot may also occur following dissemination of the bacteria to aboveground stems via insect vectors, heavy precipitation events, or hail damage. Additionally, early in the growing season, low oxygen conditions caused by compaction of soil and/or a high level of precipitation can lead to decay of infected tubers and non-emergence.

2.2. Study area

The study focused on a seed potato field experiment located in Lelystad, the Netherlands, where six different seed potato cultivars, known to exhibit variation in traits (including the growth rate), were sown at the end of May 2022 (week 21, Fig. 2 and Table 1) at the planting distance of 0.5 m. Prior to sowing, blackleg, a bacterial disease that causes soft rot and blackening of potato stems, was introduced to tubers through vacuum-infiltration with *D. solani* (IPO2222), *P. atrosepticum* (IPO1007) and *P. brasiliense* (IPO3649) suspended in water (van der Wolf et al., 2017). Two concentrations of inoculum were used depending on the level of susceptibility of a given cultivar we observed in past field experiments (Table 1). Specifically, higher concentrations were applied to Kuros and Kuroda cultivars since the lower inoculum concentration in previous trials resulted in few successful infections. This ensured a more realistic evaluation of disease response across cultivars, preventing uncharacteristically strong expression of symptoms and excessive mortality in susceptible cultivars should the concentration be increased uniformly whilst achieving higher infection rates in the more resistant cultivars. The growing season was characterised by warm weather with limited rainfall events (a weather chart is available in the Supplementary Material) that were supplemented with irrigation following standard management practices for clay soil present in the study area.

Following the plant emergence, visual health inspections of all plants were performed by a crop disease expert from the Dutch General Inspection Service (NAK); these were conducted prior to each data acquisition on 13.06.2022, 28.06.2022, 04.07.2022, and 11.07.2022. All plants with visual symptoms were physically labelled in the field and had their locations measured with RTK GNSS positioning. Plants, which had developed visual symptoms within the subsequent week were subsequently classed as presymptomatic. In the case of an infection-induced die-off, an annotation was only retained if plant material was still remaining aboveground. The breakdown of disease prevalence in each of the varieties is shown in Table 2.

Fig. 1. Examples of blackleg disease symptoms in potato plants including initial leaf wilting and chlorosis, stem die-off, and whole plant die-off.

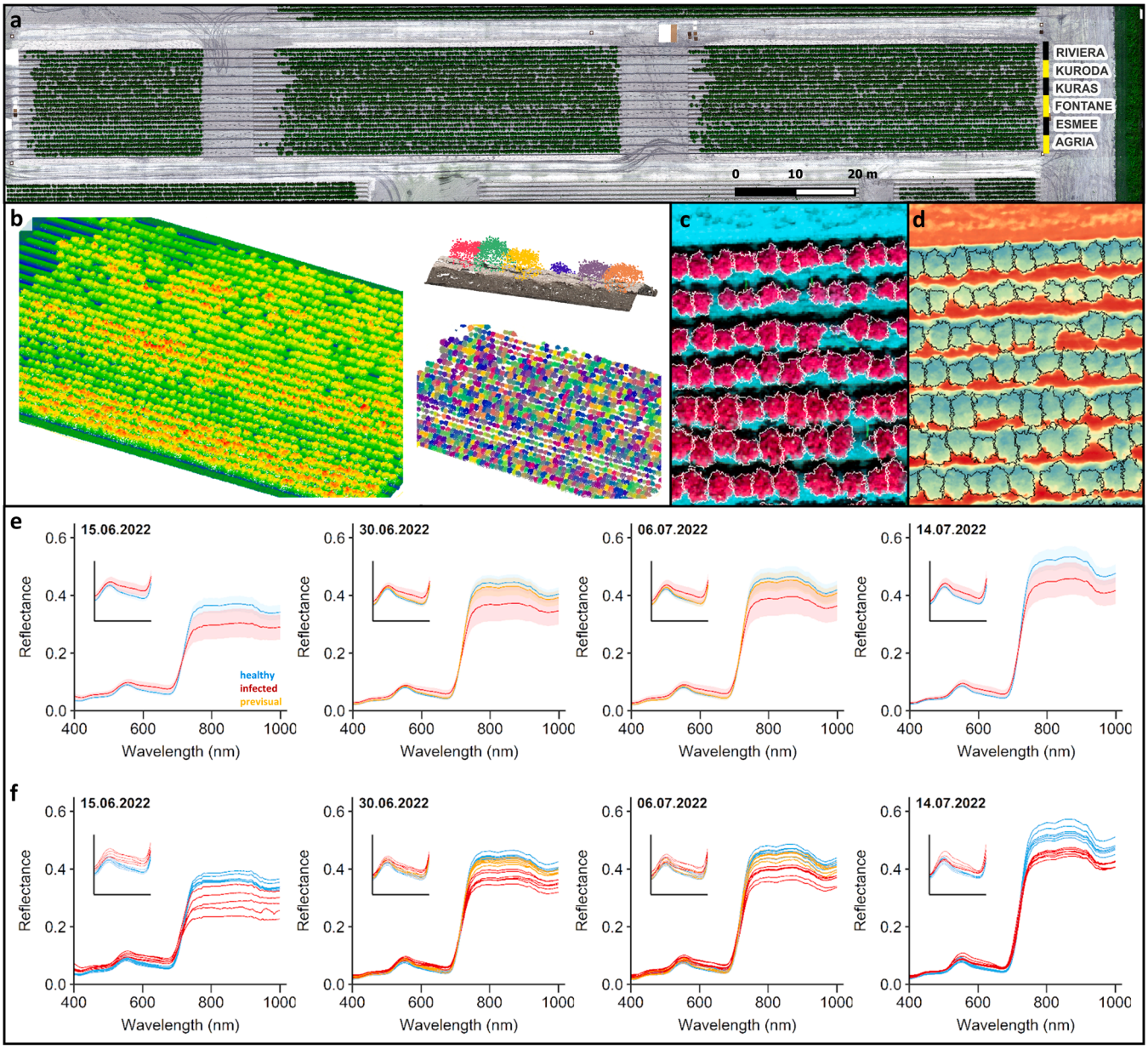

Fig. 2. (a) Layout of the experimental field used in the study with six seed potato cultivars sown across four rows and three blocks each. (b-d) Example subsets of UAV LiDAR (b), hyperspectral (false colour composite, c) and thermal data (d) collected on 30.06 with individual plant segmentation results. (e-f) Average spectral signatures of healthy (blue), presymptomatic (orange) and symptomatic (red) plants affected by blackleg based on samples from all cultivars (e) combined and (f) separated where the mean for each cultivar is represented by a single line; graph insets highlight changes in the 500–700 nm regions, whilst colour shading in (e) represents one standard deviation.

Table 1
Background information on the utilised seed potato cultivars, including the level of susceptibility to blackleg as provided by Agrico seed potato distributor on a scale from 1 (highly susceptible) to 10 (highly resistant) and average successful infection rates achieved in past experiments based on inoculation of 5400 tubers with *D. solani* (IPO2222), *P. atrosepticum* (IPO1007-IPO1012) and *P. brasiliense* (IPO3649- IPO3654).

Cultivar	Crop type	Blackleg susceptibility level	Past inoculation success rate	Typical aboveground infection symptoms	Inoculum concentration
Agria	First early	5 – Susceptible	54.6 %	Apparent: yellowing, wilting and desiccation of leaves and stems	CFU $10E^5$ ml^{-1}
Esmee	Second early	7 – Slightly susceptible	49.6 %	Apparent: yellowing, wilting and desiccation of leaves and stems	CFU $10E^5$ ml^{-1}
Fontane	Mid-late	6 – Slightly susceptible	44.4 %	Subtle: stem softening and striping, which may lead to dieback	CFU $10E^5$ ml^{-1}
Kuras	Maincrop	5 – Susceptible	2.9 %	Subtle: stem softening and striping, which may lead to dieback	CFU $10E^6$ ml^{-1}
Kuroda	Mid-late	6 – Slightly susceptible	5.0 %	Very subtle: dieback can be restricted to a single stem	CFU $10E^6$ ml^{-1}
Riviera	First early	5 – Susceptible	26.0 %	Moderately apparent: stem softening and plant lodging	CFU $10E^5$ ml^{-1}

Table 2
Blackleg prevalence across investigated seed potato cultivars based on the NAK inspections, showing a breakdown of symptomatic (INF), presymptomatic (PRES) and healthy (HLT) plants for four UAV data acquisition dates. Note: the total number of plants across dates may differ due to die-off and late emergence.

Date	15.06.2022			30.06.2022			06.07.2022			14.07.2022		
Cultivar	INF	PRES	HLT	INF	PRES	HLT	INF	PRES	HLT	INF	PRES	HLT
Agria	1	n/a	1227	105	19	1106	119	20	1086	129	n/a	1085
Esmee	4	n/a	1219	41	56	1111	102	59	1052	153	n/a	1052
Fontane	18	n/a	1189	174	35	991	201	28	963	213	n/a	963
Kuras	0	n/a	1193	56	13	1115	70	9	1115	76	n/a	1115
Kuroda	6	n/a	1158	41	28	1099	71	16	1083	85	n/a	1083
Riviera	4	n/a	1211	60	103	1053	161	78	975	228	n/a	975
All	33	n/a	7197	477	254	6475	724	210	6274	883	n/a	6273

2.3. UAV data acquisition and preprocessing

Three different sensor modalities (hyperspectral, LiDAR, thermal) expected to be sensitive to physiological responses to blackleg infection were explored in this study. For this purpose, UAV multimodal data was acquired on four occasions across the growing season in weeks 24, 26, 27 and 28 (on 15.06.2022, 30.06.2022, 06.07.2022 and 14.07.2022), covering plant establishment, tuber initiation and tuber bulking growth stages. Hyperspectral and LiDAR data were acquired with a co-aligned Headwall Nano Hyperspec VNIR imager and a Velodyne VLP-16 LiDAR sensor onboard a DJI M300 RTK platform flown within 2 h of the solar noon in sunny and dry conditions, whereas thermal imagery was acquired shortly afterwards with the use of FLIR Tau 2 camera onboard a DJI M210 RTK platform that was coaligned with a Hi-phen multispectral camera to aid photogrammetric reconstruction of thermal orthomosaics within Agisoft Metashape. A full breakdown of all sensors and flight parameters is provided in Table 3 whilst representative snippets of the acquired data are shown in Fig. 2.

All data was radiometrically calibrated and georeferenced following procedures most appropriate for a given sensor. Hyperspectral imagery was corrected with the use of a 3 × 3 m calibration target with three reflectance levels (11 %, 30 % and 56 %) deployed in the field, spatially down sampled by a factor of 2, and spectrally smoothed with a Savitzky-Golay filter (1st order polynomial with a window size of 11) from the 'hsdar' package in R. The thermal orthomosaics were empirically corrected based on field measurements of four 60×60 cm wooden targets painted in different shades to create thermal contrast; field reference measurements were obtained with the use of a handheld infrared radiometer (Raytek Raynger ST) immediately after the thermal UAV overflight. Direct georefering relying on flight trajectory and platform movements information from an Applanix APX-15 GNSS/IMU was applied to hyperspectral and LiDAR data, whereas for thermal and RGB imagery 5–7 Ground Control Points (GCPs) were used.

In addition to the multimodal data, high spatial resolution UAV RGB imagery was acquired early in the season following plant emergence (on 15.06 in week 24) and processed into a point cloud within Agisoft Metashape to allow identification of exact locations of each individual potato plant and extraction of ridges onto which the seed potatoes were sown. To achieve this, points belonging to vegetation and ridges were separated using Support Vector Machine (SVM) classification based on RGB digital numbers. The ridge point cloud was used as a reference for registration of subsequent LiDAR data utilising the 3D iterative closest point (ICP) surface matching algorithm employed within CloudCompare. Following the registration, all LiDAR point cloud heights were normalised based on a DTM derived from the RGB point cloud.

Table 3
Breakdown of sensors deployed in this study and key acquisition details.

	Headwall Nano Hyperspec VNIR	Velodyne VLP-16	FLIR Tau 2	Hi-phen Airphen	DJI Zenmuse P1
Sensor type	Pushbroom imaging spectrometer	LiDAR	Microbolometer thermal camera	Multispectral camera	RGB camera
Focal length	12 mm	n/a	19 mm	8 mm	24 mm
Spectral range	400–1000 nm	903 nm	7.5–13 um	450–850 nm	RGB
Number of bands	270	n/a	1	5	3
Platform	DJI M300 RTK	DJI M300 RTK	DJI M210 RTK	DJI M210 RTK	DJI M300 RTK
Flight height	30 m	30 m	30 m	30 m	20 m
Flight direction	East-West	East-West	East-West	East-West	East-West
Number of flightlines	7	7	6	6	6
Ground sampling distance	1.3 cm	n/a	2.7 cm	1.7 cm	0.25 cm
Acquisition days	15.06.2022, 30.06.2022, 06.07.2022, 14.07.2022	15.06.2022, 30.06.2022, 06.07.2022, 14.07.2022	30.06.2022, 06.07.2022, 14.07.2022	30.06.2022, 06.07.2022, 14.07.2022	15.06.2022

2.4. Individual plant delineation and extraction of plant-level metrics

Individual plants were delineated on each acquisition day by applying Dalponte segmentation from 'lidR' package in R to Canopy Height Models (CHMs) obtained from normalised LiDAR point clouds with plant centroids used as initial seeds (Fig. 2b). Prior to CHM calculation, all ground points were removed from the datasets. Additionally, to ensure no noisy points between ridges were retained, masks based on hyperspectral imagery were applied. The cut-off values were consistent across all datasets: an OSAVI value of 0.3, separating vegetation from soil, and a reflectance value of 2 % at 800 nm eliminating shadows; the same masks were applied to both hyperspectral and thermal imagery. The resultant point clusters were converted into plant polygons by fitting a concave hull to their extents.

For each delineated plant, average spectral signatures and 131 multimodal metrics were computed. In the case of hyperspectral imagery, these included a range of commonly applied vegetation indices sensitive to variations in pigment concentration and biomass. For LiDAR, the features were related to canopy structure, volume, or area. Whereas in the case of thermal imagery temperature-based metrics, including Crop Water Stress Index (CWSI), were computed. The full list of derived metrics and associated sources is available in the Supplementary Material. The CWSI was derived based on the image values, utilising the 2nd and the 98th percentile of canopy temperatures within the experimental field as fully-transpiring non-transpiring baselines.

2.5. Symptoms expression across diseases, cultivars and modalities

We explored the effect of infection on the acquired metrics across different cultivars by using Linear Discriminant Analysis (LDA), which aims to maximise the ratio of between-class variance to within-class variance, thereby enhancing class separability in a lower-dimensional space. Subsequently, Random Forest (RF) was employed to assess the relative importance of these metrics in differentiating infected from non-infected plants.

Application of LDA aimed to visually highlight the differences between varieties, the separability of different infection stages, and the differentiation power of a given modality. For this purpose, three set-ups were employed for each modality separately, contrasting the healthy plants against symptomatic and presymptomatic blackleg cases. To provide generalised insights, data from acquisitions with all modalities (i.e. from 30.06, 06.07 and 14.07) were utilised following pareto scaling normalisation that was applied to each day. Additionally, Principal Component Analysis (PCA) transformation was applied to each of the modalities due to the large number of metrics, many of which were highly correlated. LDA was then performed on PCA-transformed inputs: 30 principal components (PCs) for hyperspectral and LiDAR metrics and 3 for thermal metrics, explaining >99.9 % of variation within the data.

To gain deeper insights into the relative importance of metrics across all modalities, we employed RF analysis. Separate RF models were built for each acquisition day (30.06, 06.07 and 14.07) by combining data from all modalities (hyperspectral, LiDAR, thermal). Feature importance scores were then extracted for each metric to quantify its contribution in differentiating infected from healthy plants. To mitigate potential biases introduced by highly correlated metrics, a pre-processing step involved removing features exhibiting Pearson correlation coefficients exceeding a threshold of 0.9. The RF models were built with 500 trees, where each tree considered a random subset of 9–15 features (depending on the tuning outcome) at each split during its construction. The importance of a metric was assessed based on the decrease in Gini impurity it caused when used to split a node. The final importance score for each metric was obtained by averaging its importance across all trees in the forest. This approach provides a robust assessment of which metrics, after addressing collinearity, contribute most significantly to differentiating infected from healthy plants within the combined modalities, for each acquisition day.

2.6. Infection detection capabilities and model transferability

We implemented linear Support Vector Machine (SVM) classification algorithms to identify diseased plants on different acquisition days, and subsequently evaluated how their performance varies across potato cultivars and different combinations of modalities under the assumption that incorporating information from different modalities would provide an advantage in disease incidence identification. Separate models were developed for each of the acquisition days (30.06, 06.07 and 14.07) according to four modality set-ups, respectively containing: (i) H - hyperspectral, (ii) HL - hyperspectral and LiDAR, (iii) HT - hyperspectral and thermal, (iv) HLT - hyperspectral, LiDAR and thermal metrics. Data from all cultivars were used for this purpose, with an 80:20 split for training and testing - the split was applied to each cultivar separately to ensure equal representation; presymptomatic infections were included in the healthy class for modelling purposes. Class weighting was applied to account for the severe imbalance between the healthy and infected classes.

We fitted each model on the training sample using the 'e1071' package in R following hyperparameter tuning performed on each input dataset, and subsequently assessed classification accuracy for each cultivar separately and collectively for all cultivars. Two separate approaches for confusion matrix derivation were used with detected presymptomatic cases either treated as (i) healthy specimens to test the reproducibility of the inspector's assessment (false positives) or as (ii) true infection detections allowing early plant removal (true positives). The developed models were also tested on other available acquisition days to assess their robustness and transferability across the growing season; the accuracy metrics were similarly calculated collectively for all cultivars, and for each cultivar separately.

3. Results

3.1. Potential of different modalities for blackleg detection

Principal Component Linear Discriminant Analysis (PC-LDA) allowed exploring the overall identification power that each of the utilised modalities might offer, highlighting hyperspectral domain as most important for late blackleg identification throughout the growing season (Fig. 3). Spectral metrics not only offered clear separation between the healthy and infected plants, but also allowed capturing changes in the presymptomatic stage of infection. However, the level of separability for presymptomatic infections varied depending on the day of data acquisition, with the strongest responses observed on 30.06 (see Supplementary Material for PC-LDA biplots for separate acquisitions).

Whilst hyperspectral domain offered clear separation between the healthy and infected plants, the response in the structural and thermal metrics was not as pronounced; this is evident by the substantial overlap between classes along both axes of the PC-LDA (Fig. 3). Thermal imaging, although showing least discrimination power among the investigated modalities, was able to capture presymptomatic infection responses. However, similarly to the hyperspectral domain, large variations in the level of separability occurred across the season. PC-LDA performed on thermal metrics from 06.07 showed no separation from healthy plants (see Supplementary Material). In contrast, earlier in the season (on 30.06), clear differences in thermal responses were present. Since presymptomatic infection was also evident in structural metrics on this date, the observed increase in canopy temperature could be partly due to the smaller plant size caused by stunted growth, resulting in less transpiring plant material.

RF feature importance analysis similarly highlighted the hyperspectral domain as key for identification of infected plants (Fig. 4a). In particular, indices sensitive to the carotenoid concentration in the leaf, i.e. Photochemical Reflectance Index (PRI) and Plant Senescence Reflectance Index (PSRI), were consistently highly ranked throughout the season (Fig. 4a). PRI is a narrow-band index that targets xanthophyll

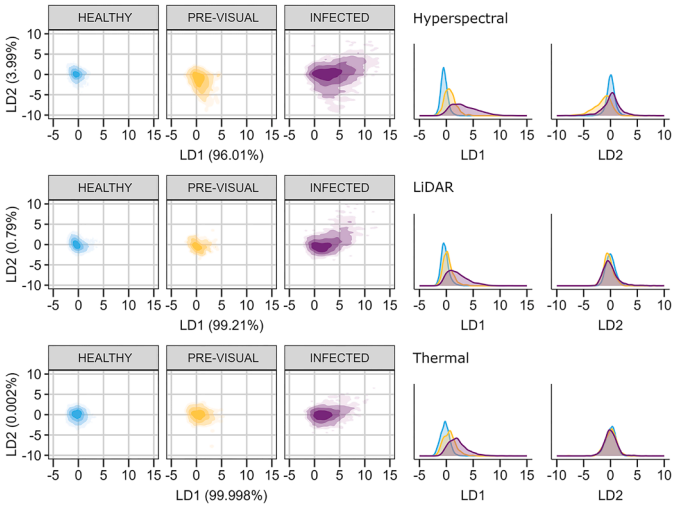

Fig. 3. Principal Component (PC) Linear Discriminant Analysis (LDA) biplots (*left*) with corresponding density distributions (*right*), visualising the separation between healthy, presymptomatic and infected potato plants based on PC-transformation of 76 hyperspectral (*top*), 52 LiDAR (*middle*), and 3 thermal (*bottom*) metrics from30.06, 06.07 and 14.07. The biplots contain over 19.000 data points, with graduated colours indicating the 50 %, 80 %, 95 % and 99 % density contours.

pigments, which play a crucial role in light absorption and dissipation during photosynthesis, therefore being indicative of a plant's photosynthetic efficiency. In contrast, PSRI primarily detects the shift in the ratio between chlorophyll and carotenoid pigments as leaves undergo senescence. We observed a clear response in the PSRI value on each acquisition date upon the onset of visual symptoms, with index values converging following prolonged (>1 week) disease manifestation (Fig. 4b). The structural index, WDVI, also showed clear responses following the development of visual symptoms (Fig. 4c). Its importance increased throughout the season as plants developed, likely reflecting both the changes in vitality and structure resulting from stunted growth and/or wilting, which were also captured by LiDAR metrics (Fig. 4d).

3.2. *Spectral changes in response to infection across cultivars*

A closer inspection of spectral responses after infection revealed substantial variation between investigated cultivars. The most prominent response was a significant drop in reflectance throughout the NIR region, observed in plants at all growth stages (Fig. 2e). However, the magnitude of this decrease varied between cultivars (Fig. 2f), with Kuroda and Riviera showing the weakest response. The variation between infected plants of different cultivars was most pronounced early in the season, gradually converging as plants matured (Fig. 2f). This likely reflects differences in developmental rates among the cultivars. A decrease in reflectance in the NIR region, though subtle, was also present in presymptomatic infections (Fig. 2e–f). The Riviera cultivar was the sole exception, exhibiting no changes in the NIR region but instead

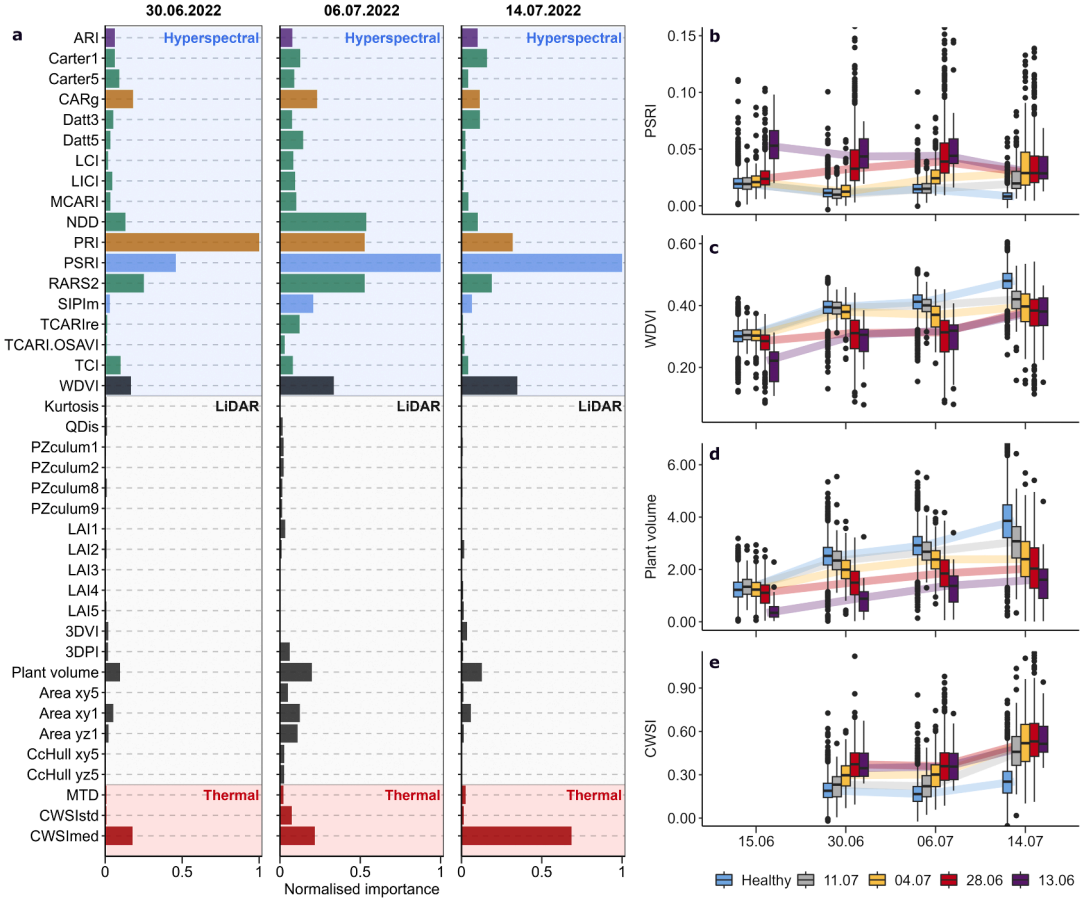

Fig. 4. (a) Normalised importance of metrics derived from hyperspectral, LiDAR and thermal data based on Random Forest's decrease in Gini impurity across different acquisition days. Bar colours indicate metric's primary sensitivity: anthocyanins – purple, chlorophylls – green, carotenoids – orange, chlorophyll to carotenoid ratio – blue, plant biomass/structure – grey, transpiration – red. For more details on the individual metrics refer to the Supplementary Material. (b-e) Impact of blackleg on selected plant-level metrics over the growing season, grouped according to the date of identification of first visible symptoms of infection; shaded connections between median values of each category provide a visual indication of the metric development trends.

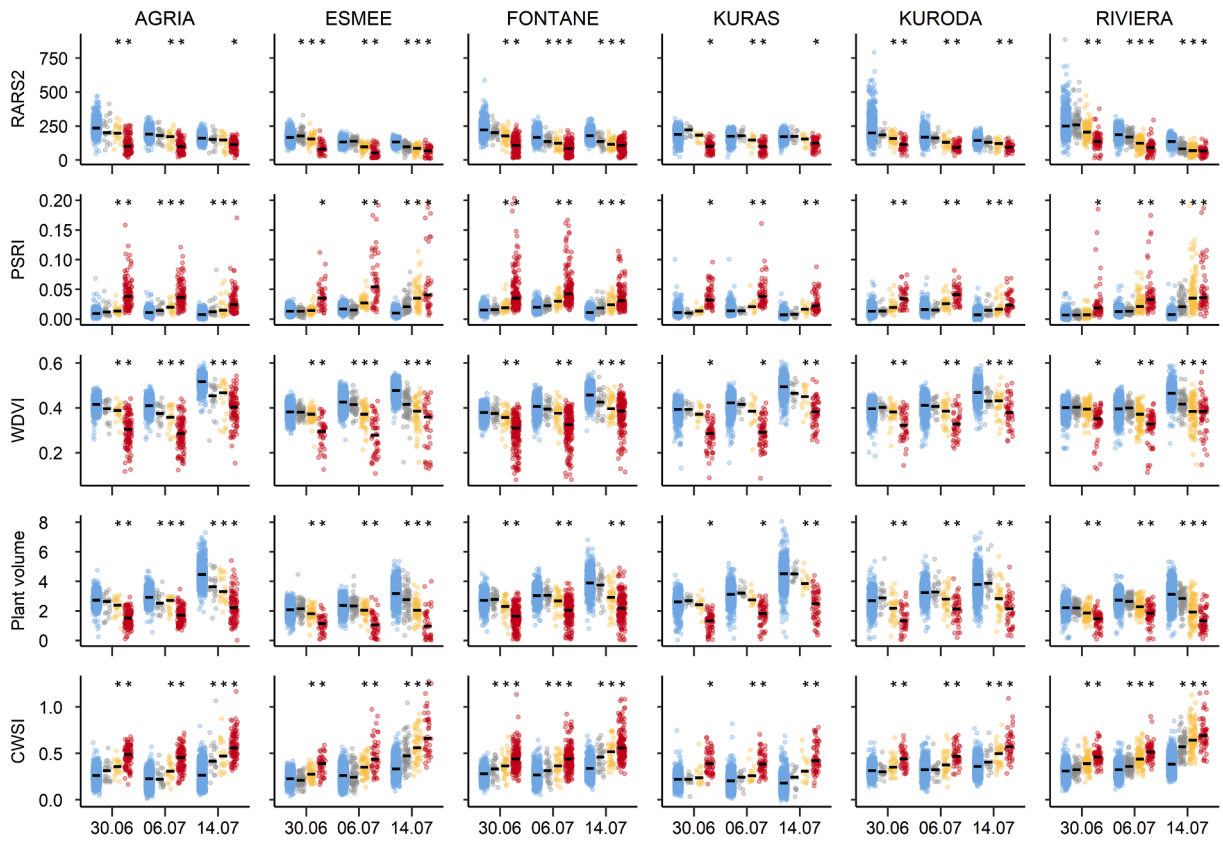

Fig. 5. Jitter plots illustrating the distribution and the median of selected plant-level metrics over the growing season for each investigated potato cultivar. Data points were grouped according to the date of identification of first visible symptoms of infection: red – observed on 13.06 or 28.06, yellow – observed on 04.07, grey – observed on 11.07, blue – healthy. Significant differences between the healthy and infected plants are indicated by a single star (*) based on Mann-Whitney U test, $p < 0.01$.

showing a minor reflectance decrease across the 550–650 nm range. Significant spectral changes in response to infection could also be observed in one of the chlorophyll absorption regions (550–680 nm), and, in some cultivars, in the carotenoid absorption region (500–550 nm). This suggests that vegetation indices linked to photosynthetic activity, carotenoid content, and chlorophyll concentration could provide valuable diagnostic information.

While chlorophyll-based indices showed promise, their applicability in generalised models might be limited since the spectra lacked the typical responses observed in shorter wavelengths, typically used for these indices, that reflect changes in chlorophyll content. Additionally, inherent physiological differences between cultivars contributed to spectral variation even among healthy specimens, leading to occasional overlaps with infected plants from other cultivars; this overlap was most evident early in the growing season (Fig. 2f). The varying importance of indices targeting chlorophyll was reflected in the RF feature importance analysis, being highly important on 06.07 but contributing much less on the other two acquisition days (Fig. 4a). On 06.07, chlorophyll indices' values were most consistent across different cultivars and showed significant differences between infected and healthy plants as shown on Fig. 5 with Ratio Analysis of Reflectance Spectra (RARS2) that combines reflectance values from the red and the red edge regions. The separability between healthy, symptomatic and presymptomatic infection stages varied between the utilised cultivars, with latterly symptomatic plants showing little response in the case of Agria and Kuras and substantial shifts for other cultivars. Similar patterns could be seen in other indices (see Fig. 5), with both the separability and the range of measured values substantially varying across cultivars. Whilst clear responses in the presymptomatic stage could be captured in some cultivars (e.g. WDVI in Agria), in others, even symptomatic stages did not initially manifest (e.g. WDVI in Kuras).

PCA-LDA analysis of vegetation indices derived from hyperspectral data (Fig. 6) confirmed the observed cultivar-specific differences in terms of both separability between the healthy and infected classes, and the strength of stress responses. The Riviera cultivar displayed a distinct pattern, but still achieved separation from healthy plants. Responses in other cultivars were more similar, with Fontane and Kuroda showing the least separation despite having vastly different susceptibility levels (Fontane – high, Kuroda – low). Although the analysis indicated limited to no separability between healthy and presymptomatic plants, we observed substantial shifts in LD1 values for most cultivars (except Kuras) on 30.06 (see Supplementary Material). This suggests presymptomatic detection might be more achievable at earlier plant growth stages.

3.3. *Symptoms expression in thermal and LiDAR domains*

Even though the response in thermal and LiDAR domains was not as pronounced, they provided valuable information on disease effects on plant development and functioning. Throughout the season we could observe clear reduction in plant volume following disease manifestation; the longer the visible symptoms were present, the higher the overall reduction in plant volume (Figs. 4d and 5), which can be attributed to both stunted growth and dieback. However, this reduction in symptomatic plants relative to the healthy population was inconsistent both across cultivars and over time. The clearest signal in newly infected plants was observed during the early growth stages, resulting in 33–45 % median reduction in plant volume on 30.06 compared to 7–17 % reduction on 06.07 and none to 19 % reduction on 14.07 when only susceptible cultivars that were more likely to suffer from dieback were

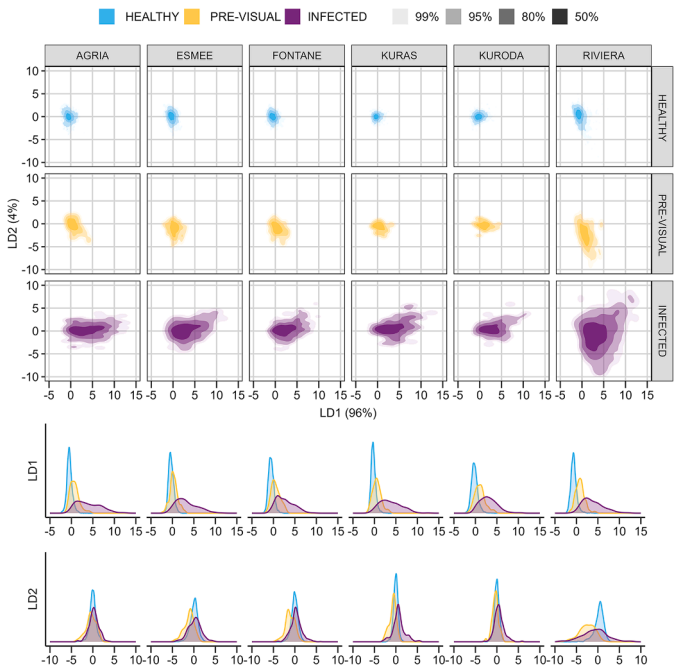

Fig. 6. Principal Component (PC) Linear Discriminant Analysis (LDA) biplots for each investigated potato variety showing density distribution for healthy, presymptomatic and infected potato plants based on PC-transformation of 76 hyperspectral metrics from 30.06, 06.07 and 14.07. The biplots contain over 19.000 data points,with graduated colours indicating the 50 %, 80 %, 95 % and 99 % density contours.

affected (i.e. Agria, Esmee, Riviera, Fig. 5). Varying growth patterns, regardless of infection, further amplified differences between cultivars as the growing season progressed (Fig. 7). For example, the relative difference in healthy plant volume between two most different cultivars (Riviera and Agria) increased from 0 % to 40 % between 15.06 and 14.07. The latter entered the flowering stage already on 06.07, whilst the former on 14.07 was yet to start flowering; the Esmee cultivar similarly developed more slowly and was still in the tuber initiation phase when the data collection ceased. While only plant volume is presented here for illustrative purposes, other structural metrics showed similar variability across cultivars.

We observed similar potential difficulties in utilisation of CWSI, even though significant canopy temperature, and consequently CWSI value, increase followed infection across all growth stages and cultivars (see Figs. 4e and 5). Significant canopy temperature increase in the pre-symptomatic plants could even be captured early in the season for most cultivars (except for Kuras that proved resistant to the employed blackleg strains), highlighting the applicability of utilising thermography for capturing early responses. Still, the importance of CWSI, based on the RF analysis, varied considerably throughout the season, showing relatively low importance on 30.06 and 06.07 and then becoming the second most important feature on 14.07 when the canopy temperature differences between healthy and infected plants were most pronounced (Fig. 4a). This could be attributed to large variability in the CWSI value across cultivars, restricting the usefulness of this metric for blackleg identification. For example, the median CWSI value ranged from 0.18 to 0.38 for the healthy and from 0.40 to 0.64 for the infected plants (Fig. 7). In particular, the Kuroda cultivar significantly deviated from others, with its plant canopies being increasingly cooler over the season. This, akin to LiDAR metrics, highlights the difficulty in obtaining universally applicable metrics where absolute values, even from a single acquisition date, can provide sufficient interpretative power.

3.4. Disease detection capabilities across modalities

We proceeded to investigate whether robust disease detection models utilising obtained metrics could still be developed despite the challenges associated with variability in plant responses and the limitations of individual metrics highlighted in previous sections. The impact of utilising different modality combinations at different growth stages within SVM models is shown in Table 4. High detection rates could be achieved across all scenarios, ranging from 81 % to 89 %, with small variations between modality combinations. No consistent patterns emerged, though LiDAR inclusion proved beneficial during the early growth stage, leading to an increase in the detection rate of 4 %, reflective of the larger and more consistent impact on plant structure across cultivars. Similarly, additional modalities typically led to small improvements (1–4 %) on other days with HLT showing best performance. Although instances of falsely identified infections (false positives) substantially exceeded those of missed infected plants (false negatives), a significant portion of the misclassified plants belonged to the presymptomatic infection stage. When considered to be True Positives, precision ranges increased from 71–76 % to 83–86 % on 30.06 and from 72–81 % to 75–84 % on 06.07, demonstrating comparable values across different acquisition days.

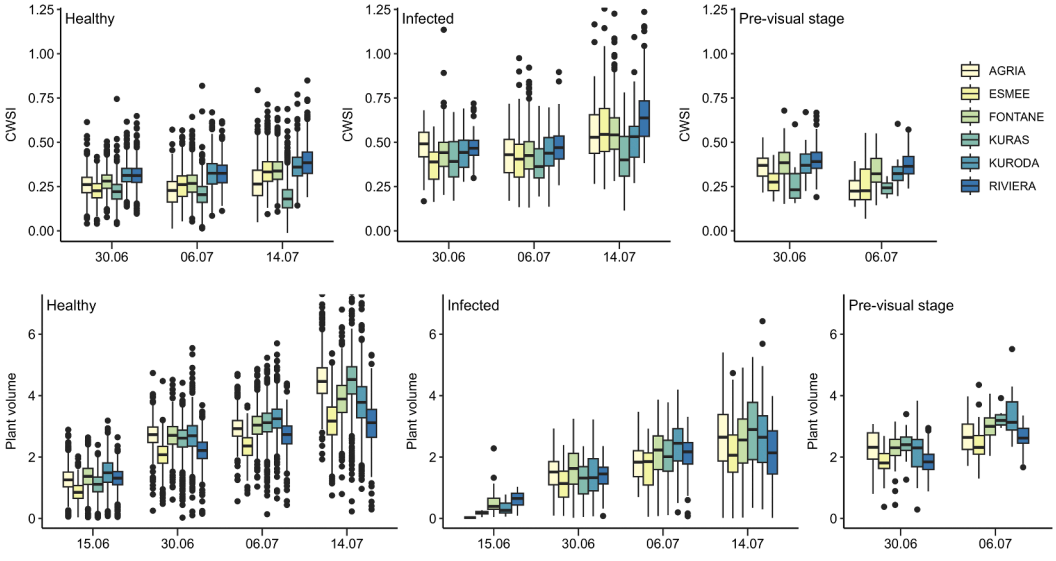

Fig. 7. Comparison of CWSI (top) and plant volume (bottom) values across different seed potato plants.

Table 4
Achieved blackleg detection rates of the developed models utilising metrics extracted hyperspectral (H), LiDAR (L) and/or thermal (T) data with presymptomatic detections treated as false positives/true positives (only available for 30.06 and 06.07). Best performing models are shown in bold.

	30.06			06.07			14.07		
Mode	Recall	Precision	Bal. Acc.	Recall	Precision	Bal. Acc.	Recall	Precision	Bal. Acc.
H	83.8/84.8	72.0/84.0	90.3/91.8	85.0/85.5	81.2/84.4	91.4/91.8	80.8	81.3	89.1
HL	**87.4/89.1**	**71.0/84.1**	**92.5/93.9**	85.7/86.2	79.2/82.4	91.6/92.0	81.9	82.9	89.8
HT	81.6/83.3	76.3/86.0	90.0/91.2	85.0/85.5	79.6/82.8	91.3/91.7	73.3	91.7	86.4
HTL	81.6/83.2	74.7/83.2	89.9/90.1	**87.1/87.6**	**71.9/75.3**	**91.6/92.1**	**84.7**	**81.1**	**91.0**

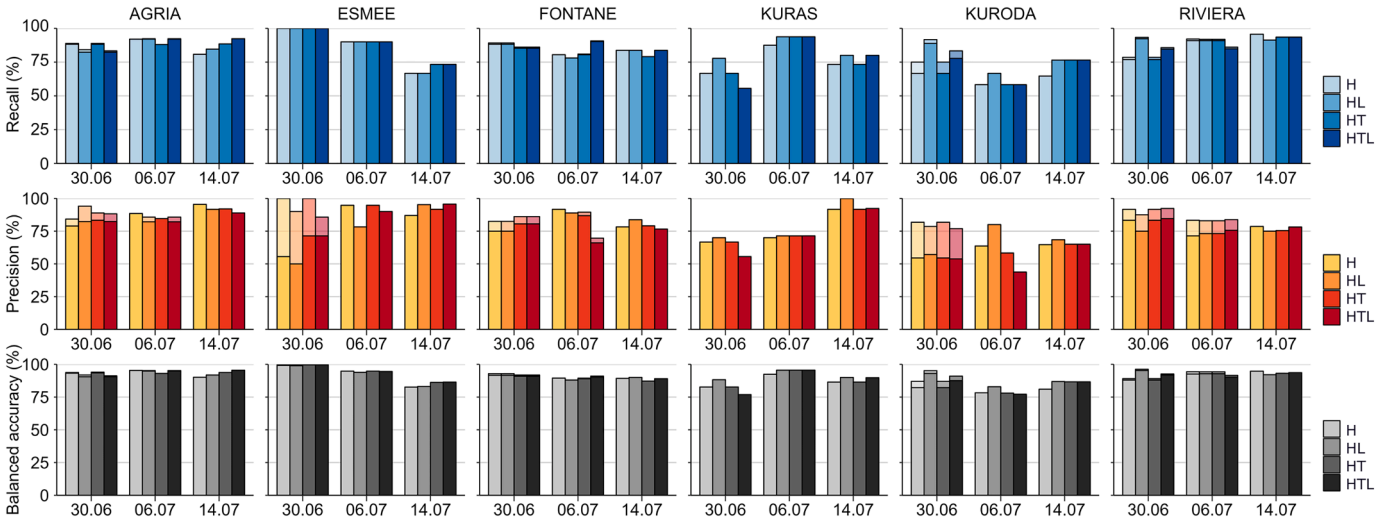

Fig. 8. Achieved blackleg detection rates of the developed models for each variety utilising metrics extracted from hyperspectral (H), LiDAR (L) and/or thermal (T) data with presymptomatic detections treated as false positives (solid fill) and true positives (semi-transparent fill).

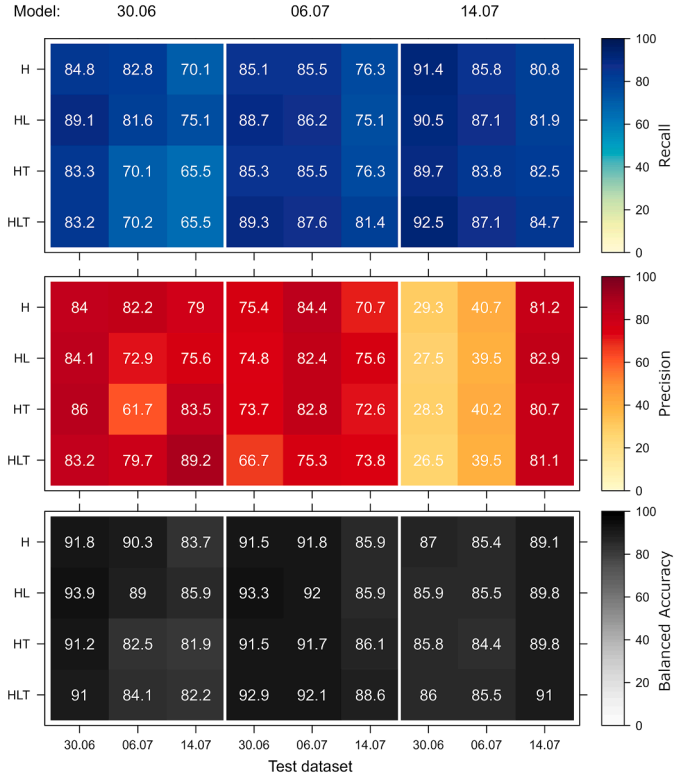

Fig. 9. Transferability of single-day SVM blackleg detection models, showing achieved recall (*top*), precision (*middle*) and balanced accuracy (*bottom*) on test datasets from different acquisitions. Four combinations of modalities were tested utilising metrics extracted from hyperspectral (H), LiDAR (L) and/or thermal (T) data. In all cases presymptomatic detections were treated as True Positives.

Despite achieving a high collective disease detection rate, we observed significant discrepancies and inconsistencies across the investigated cultivars (Fig. 8), with only three (Agria, Fontane, and Riviera) showing comparable detection rates across all acquisition days. The inclusion of presymptomatic detections improved cultivar-specific precision rates (Fig. 8), most significantly in Esmee and Kuroda on 30.06 when the trained models were able to identify up to 15 %/43 % of all presymptomatic infections (Esmee/Kuroda), leading to increases in precision from 60–71 % and 54–57 % to 86–100 % and 77–82 %, respectively. The weaker performance observed in the Kuroda cultivar aligns with previous investigations of individual domains, which revealed lower spectral separability, less pronounced canopy temperature increases, and subtler structural changes compared to other cultivars. Similarly to the collective analysis, no definitive patterns emerged regarding the optimal modality combination. Although the differences in performance tended to be small, the use of hyperspectral and LiDAR metrics appeared to offer the most consistent detection rates. This combination demonstrated the most promising results early in the season when we observed significant improvements in detection rates of 11–17 % over the sole use of hyperspectral metrics in cultivars with subtler symptoms (i.e. Kuras, Kuroda and Riviera).

3.5. *Detection model transferability across the growing season*

We further tested the robustness of the single day models through their application across the different acquisition days (Fig. 9), showing that models trained on early growing season data (30.06) could be directly transferred to later dates with success depending on the choice of modalities. The combination of hyperspectral and LiDAR (HL) data remained the most consistent, achieving recall rates of 82 % on 06.07 and 75 % on 14.07. In contrast, models incorporating thermal information exhibited rapid decline in performance, with recall dropping from 83 % on June 30th to 70 % on July 6th and 66 % on 14.07. This

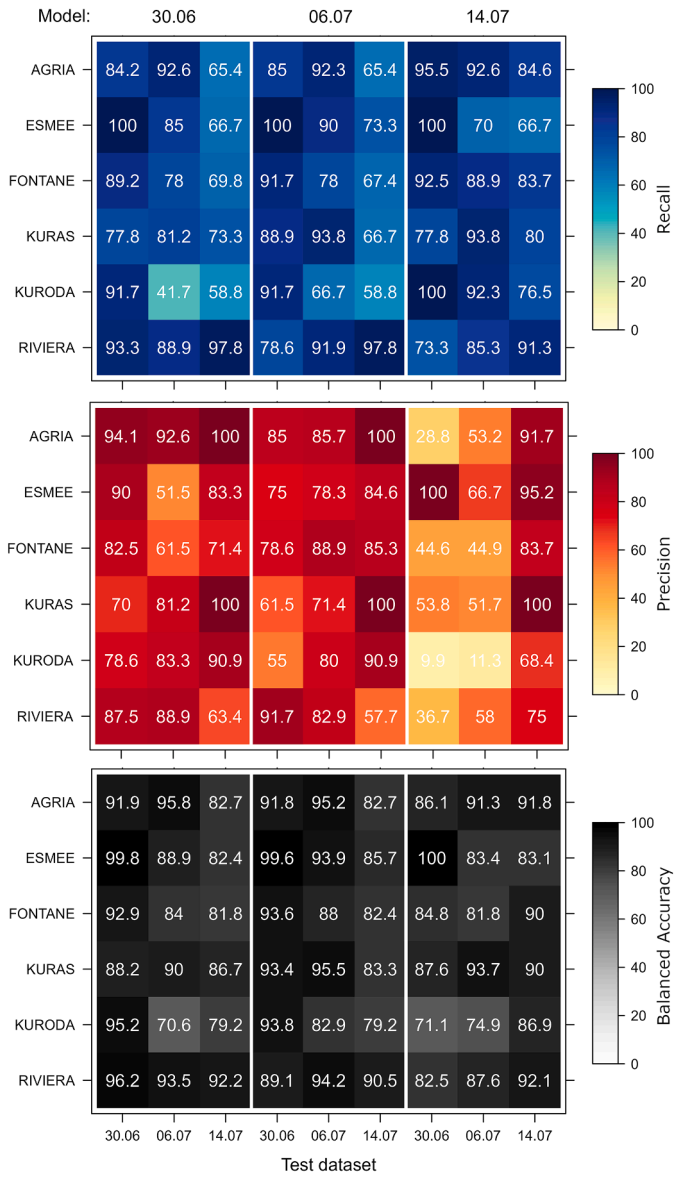

Fig. 10. Transferability of the HL SVM blackleg detection model utilising hyperspectral and LiDAR metrics, showing achieved recall (*top*), precision (*middle*) and balanced accuracy (*bottom*) on test datasets from different acquisitions. In all cases presymptomatic detections were treated as True Positives.

decline was not present in 06.07 models that incorporated thermal information, which can be attributed to its diminishing importance relative to other metrics for classification since the thermal stress signal became weaker and more variable across the cultivars (see Figs. 4a, 5 and 7).

All models developed on 14.07 transferred poorly to the earlier season. Although very high recall could be achieved (84–93 %), incorporating samples from different cultivars that were at different growth stages significantly affected the overall performance leading to persistent misclassification of healthy plants (precision rates of 27–41 %). Some of the cultivars utilised in training were in the tuber initiation stage (Riviera and Esmee), while others were flowering (Agria, Kuras, and Kuroda) or already in the tuber bulking stage (Fontane), which affected the specificity of responses we observed in the derived metrics. The weakest performances were indeed recorded in cultivars, which experienced substantial shifts in the development between the acquisition days (Fig. 10), i.e. Kuroda (from tuber initiation to end of flowering, 10–12 % precision for HL modality), Fontane (flowering to tuber bulking, 45 % precision) and Agria (53 % precision on 06.07 at peak flowering and 29 % on 30.06 during the tuber initiation). Although only the HL mode is shown here, similar patterns could be observed for other modality combinations (see Supplementary Material).

Substantial differences between cultivars in the ease of transfer were also present in earlier models (see Fig. 10 and Supplementary Material). These performed worst for least susceptible cultivars with weakest symptoms (Kuras and Kuroda) with recall on 06.07 dropping by 25 % and 13 %, respectively (based on the 30.06 HL model), due to infections with subtle symptoms being missed or healthy plants, especially with delayed emergence, being misclassified. Nevertheless, for other cultivars the performances were more consistent, with detection rates often comparable to those of the same day models. This highlights the potential for using multi-modal data and machine learning models for disease detection but also demonstrates the importance of considering cultivar-specific characteristics, i.e. growth rates and symptoms expression, when developing and applying such models.

4. Discussion

Whilst the potential of remote sensing for disease detection in crops is relatively well-established, a gap exists in understanding how cultivar and growth stage variations might influence the responses captured by different modalities, and subsequently affect disease detection capabilities. This study addressed this knowledge gap by exploring the impact of these factors on multimodal remote sensing signatures at individual plant level. Although our focus here is on blackleg in seed potatoes, the findings on specificity of responses hold broader implications for disease detection across other crops and diseases.

4.1. Linking remote sensing metrics to disease responses

Establishing clear links between observed changes in derived metrics and the expected infection symptoms is crucial for development of robust detection models as it not only improves their explainability but also ensures the observed responses are indeed caused by the stress agent in question. Blackleg can induce a range of symptoms involving development of black rot lesions within the seed tuber that spread to stems. This typically disrupts nutrient and water uptake, and can lead to yellowing due to decreased chlorophyll content, wilting, maceration and desiccation of leaves and stems (van der Wolf and De Boer, 2007).

Although chlorophyll decrease due to chlorosis and necrosis is a well-known symptom (Steglińska et al., 2022), our analysis highlighted indices relating to the xanthophyll cycle activity and the carotenoid-to-chlorophyll ratio as most valuable. Though, the importance of the derived plant-level metrics shifted throughout the season. Early on, PRI (sensitive to xanthophyll cycle activity) held the most weight, reflecting early plant stress responses. However, as the season progressed, PSRI (sensitive to the carotenoid-to-chlorophyll ratio) became more informative, indicating potential changes in pigment composition. Several studies support the link between derived metrics and photosynthesis inhibition following blackleg infection. For example, exposure of potato leaves to a culture filtrate of *Pectobacterium carotovorum* resulted in a down-regulation of psaD, which is a key component of Photosystem I (PSI) (Montesano et al., 2004). PsaD was similarly found to be down-regulated by methyl jasmonate molecules created by plants upon infection with *P. carotovorum* (Hachoud et al., 2019; Montesano et al., 2004). This down-regulation correlates with accumulation of hydrogen peroxide in chloroplast that, although being part of a plant defence response, negatively affects photosynthesis (Kovač and Ravnikar, 1994).

Whilst the connection between carotenoids (which assist with photosynthesis and light protection) and blackleg is unclear, a number of previous studies explored their role in plant pathogen interactions. Carotenoids are involved in the production of abscisic acid (ABA) by host plants, a hormone that plays a key role in plant's responses to

infection (Ton et al., 2009). Following ABA synthesis plants can respond to invasion by closing stomata upon contact with microbes to increase their resistance, as have been shown for *Pseudomonas syringae* pv. *tomato*. After penetration, the role of ABA is controversial. In *Arabidopis thaliana*, ABA repressed callose deposition, which resulted in an increased resistance to *P. carotovorum*, but it also decreased the resistance against abiotic stress conditions (Kariola et al., 2006). In contrast, Bagy et al. (2019) showed that *P. atrosepticum* may interfere with this defence mechanism after finding the total level of carotenoids to be lower in infected potato plants.

The relative importance of chlorophyll-sensitive indices, structural features and thermal metrics similarly varied over time. Structural changes affecting plant geometry, such as dieback, typically take longer to manifest as they require the disease to progress sufficiently. Consequently, the effect on structural metrics became more apparent later in the season. Though here, beyond dieback, we also observed evidence of stunted growth, which was most substantial early in the growing season. The need for sufficient dieback or growth stunting to occur explains why the investigation of metrics directly capturing structural information has so far been limited outside of a proximal or a laboratory set-up. Forestry studies utilising LiDAR point clouds to capture disease-induced defoliation are a notable exception (Smigaj et al., 2019b; Yu et al., 2021). So is a previous UAV study on blackleg that also reported shifts in LiDAR-derived metrics in infected potato plants (Franceschini et al., 2024).

In contrast, thermal responses can often precede visual symptoms, being indicative of issues with temperature regulation through transpiration. Whilst breadth of literature exists on links between leaf/canopy temperature and plant water status (Maes and Steppe, 2012; Smigaj et al., 2024), the usefulness of thermal data for disease identification in the field remains uncertain due to stomatal closure being a non-specific response that can occur due to both biotic and abiotic stress factors. Still, previous airborne canopy-level studies, which focused on orchards and forests, observed clear temperature increases following infection as a result of disease-induced disruptions to the water transport and/or progressive defoliation (Poblete et al., 2023; Smigaj et al., 2019a; Zarco-Tejada et al., 2018; Zhang et al., 2023). Blackleg similarly hinders water uptake and consequently affects transpiration by damaging the vascular system. This can lead to an increase in canopy temperature, as we were able to capture and confirm on all acquisition days. The strongest signal was observed during the last data acquisition (on 14.07), which could be attributed to several factors: cumulative reduction in leaf water content due to progressive vascular damage, wilting and desiccation of stems, stunted growth leading to less transpiring material, and the timing of the acquisition coinciding with a warm day following a dry period (2 mm of rain in the preceding 7 days with irrigation only applied later in the day) which might have amplified the differences between healthy and infected plants.

Quantification of the severity of disease visual symptoms could allow more nuanced links with remote sensing metrics to be established, offering a clearer understanding of the level of infection required for manifestation in different modalities. Whilst this was not explored here due to our reliance on disease experts from NAK who used established inspection protocols to identify diseased plants for prompt removal, such an approach would allow for the development of more granular models capable of distinguishing between early and advanced stages of infection. This would be highly relevant for diseases where other management interventions, such as targeted fungicide applications or biocontrol agents, are possible.

4.2. Specificity of disease symptoms manifestation in remote sensing metrics

While UAV-based disease detection is a promising avenue, the use of pre-selected remote sensing metrics for this purpose presents its own set of challenges. Symptom expression is a complex interplay between factors like cultivar resistance, strain virulence, and environmental conditions. The strain of pathogenic bacteria typically dictates disease spread and progression with those possessing a functional Type III Secretion System (T3SS) often being more virulent due to their ability to manipulate host defences (Büttner and He, 2009). Though, both the spread and symptoms development may be hindered or accelerated depending on the environmental conditions. For example, for *Clavibacter michiganensis* warm temperature and high relative humidity are most optimal, whilst in the case of blackleg, hot and dry weather typically prompts faster development of visible symptoms and higher plant mortality (Toth et al., 2011). These factors, together with cultivar-specific traits, can significantly impact the manifestation and severity of symptoms, making it challenging to rely on pre-established cues for definitive identification.

Cultivar-specific traits and development patterns may also affect the specificity of responses. We observed substantial differences both in spectral signatures and the extracted metrics for healthy plants of different cultivars. This aligns well with observations reported by others; Gold et al. (2020) similarly observed substantial differences in the leaf spectra of different potato cultivars. Attempts have even been made at utilising remote sensing data for in-field classification of crop or tree cultivars (Avola et al., 2019; Gava et al., 2022; Guimarães et al., 2023). This inherent variability even within a healthy population further complicates explicit symptom identification solely through remote sensing data.

Despite sufficient level of symptoms expression being key to successful identification of affected plants, field investigations into the impact of cultivar-specific traits on remote sensing signatures of diseased plants are lacking; previous investigations with multiple cultivars or varieties mainly focused on phenotyping cultivar resistance based on remote sensing metrics (Chivasa et al., 2020; Jay et al., 2020; Simões and Rios do Amaral, 2023). Indeed, in our study we observed large differences in disease symptom expression between the investigated cultivars, which consequently affected detection models' performances. For susceptible cultivars with apparent symptoms (Agria and Riviera), same-day models were able to reach 84–92 % and 91–93 % recall rates across the growing season (HL modality). However, for less susceptible cultivars (e.g. Esmee and Kuroda), model performance varied considerably (recall rates of 67–100 % and 67–92 %, respectively). Similarly, model transfer across the growth stages was more successful for cultivars with symptoms that were expressed more strongly.

The manifestation of disease symptoms in some of the investigated metrics varied not only across cultivars but also throughout the growing season. For example, while we could identify clear reductions in plant size across all cultivars early in the season due to growth stunting and/or dieback, later in the season substantial structural changes in latterly infected plants were primarily present in susceptible cultivars more prone to dieback. This highlights that the usefulness of different metrics may considerably vary over the growing season depending on the utilised cultivar. Similarly, the strength of the thermal signal varied over time and was the strongest during the last data acquisition (on 14.07). This could be attributed to several factors: cumulative reduction in leaf water content due to progressive vascular damage, wilting and desiccation of stems, stunted growth leading to less transpiring material, and the timing of the acquisition coinciding with a warm day following a dry period (2 mm of rain in the preceding 7 days with irrigation only applied later in the day) which might have amplified the differences between healthy and infected plants. Taking environmental conditions into account should therefore also be a consideration since weather favouring increased transpiration rates will accentuate differences between healthy and diseased plants (Smigaj et al., 2024).

Further research investigating the underlying physiological and biochemical mechanisms that drive such cultivar-specific responses to disease onset and their impact on remote sensing signatures is crucial for improving and increasing the explainability of remote sensing-based disease detection approaches, especially in the growing era of

Artificial Intelligence-driven (AI) methods that leverage vast amounts of input data to extract relevant features (Jafar et al., 2024; Jung et al., 2021). Whilst valuable insights can already be gained by focusing on remote sensing alone, explicitly linking these observations to physiological responses improves our understanding and allows critical assessment of the underlying decision-making processes, helps identify potential sources of error, can facilitate the development of broadly transferable disease detection models.

In this study we introduced multiple sources of variation, including seed potato cultivar diversity, data collection at multiple growth stages, and the introduction of various blackleg-causing strains, and subsequently were able to capture broad variability in responses. Though, the experiment's scope limited the investigation of whether different bacterial strains differentially impacted the extracted metrics. Addressing this challenge of variations in symptoms expression is key for development of broadly transferable detection models. Potential solutions could involve incorporating plant growth stage information and considering potential environmental stressors, e.g. through coupling with crop growth models (Berger et al., 2022), further exploration of normalisation techniques to account for inherent baseline differences between cultivars, or coupling remote sensing data with radiative transfer models (RTMs).

The use of RTMs would allow retrieval of functional plant traits for each cultivar, making detection models less dependent on raw metrics. The potential of using RTM-derived traits for detection of plant pathogens has already been demonstrated in olive and almond orchards (Zarco-Tejada et al., 2018, 2021). This approach also allowed identifying divergent responses between different stress agents, which could then be utilised for their discrimination (Poblete et al., 2021; Zarco-Tejada et al., 2021). Such differentiation is of high relevance for determining crop health status and enabling targeted interventions. However, it is important to acknowledge that it is also inherently challenging since similar symptoms can be triggered by a range of stress agents. The few other studies exploring disentangling stress agents were typically restricted to laboratory/greenhouse set-ups (Fallon et al., 2020; Gold et al., 2020; Moshou et al., 2014). Further research on the potential of multimodal approaches is therefore necessary to fully evaluate their synergy. So is the exploration of how cultivar-specific variations in symptom expression might affect the identified divergent pathways.

4.3. *The potential benefits of multimodal approaches for blackleg detection*

Each of the investigated modalities provided information about different physiological responses to blackleg onset. Although the hyperspectral domain was consistently being highlighted as most crucial for differentiation between healthy and diseased plants, LiDAR and thermal domains also carried information indicative of infection. Still, our investigations into the synergistic use of different modalities showed that similarly high detection rates could be achieved with any of the investigated combinations in single day detection models (recall 81–89 %, precision 75–86 %, balanced accuracy 89–94 %); combining hyperspectral metrics with features from other modalities only led to small increases (up to 4 %) in the detection rates. This is in contrast to the previous UAV study on blackleg that reported an increase in recall of 11 % (from 68 % to 79 %) after supplementing vegetation indices with LiDAR metrics (Franceschini et al., 2024). This discrepancy could potentially be caused by a substantially larger amount of inoculant applied to the tubers in that study, which caused more prominent manifestation of symptoms. Zhang et al. (2023) and Yu et al. (2021) similarly reported an increase in overall accuracy of 7–9 % for detection of pine wilt disease when combining UAV-based vegetation indices with thermal data. Improvements in the range of 1–8 % in overall accuracy (reaching 79–91 %) were also reported in olive and almond trees for *Verticillium dahliae* and *Xylella fastidiosa* when combining airborne hyperspectral data with solar-induced chlorophyll fluorescence and CWSI (Poblete et al., 2023). Other multimodal studies focusing on disease detection, although highlighting the significance of metrics capturing different responses (e.g. through feature importance analysis), rarely reported on the level of improvement compared to single modality (Smigaj et al., 2019b; Xu et al., 2023; Zarco-Tejada et al., 2018, 2021; Zhang et al., 2019).

In this study, the main differences in performance laid in the transferability to other dates. The combination of hyperspectral and LiDAR features showed most consistent performance, with detection rates up to 12 % higher compared to other modality combinations. Interestingly, sole inclusion of thermal metrics was in this case detrimental. Although feature importance analysis ranked CWSI as important, PC-LDA revealed that thermal domain offered the lowest distinction between different health classes. Inherent limitations of miniature UAV thermal cameras likely affected the strength and consistency of responses despite the data being acquired and processed in a way to ensure high quality as suggested in Smigaj et al. (2024). Miniature thermal cameras have low signal-to-noise ratio and are very sensitive to changing ambient conditions, leading to additional noise in the collected data (Kelly et al., 2019; Smigaj et al., 2017; Wan et al., 2021). Majority of other studies utilising thermal imagery for disease identification relied on more stable cameras and platforms. Still, we were able to capture consistent temperature increases in both infected and presymptomatic plants. Inclusion of the latter as healthy samples for model training might have introduced confusion, reducing models' sensitivity to infections on other days.

Although we observed substantial decrease in performance when transferring developed models across the datasets, we showed that some of the models developed early in the season demonstrated a reasonable level of success when applied to later growth stages despite the variability introduced by employing different cultivars. The HL SVM model developed on 30.06 was still able to identify 82 % of infections on 06.07 and 75 % on 14.07, whilst retaining comparable balanced accuracy (89 % and 86 %). This is an encouraging step towards operationalising the use of UAV-based sensing to support blackleg disease management. Currently, identification of blackleg in seed potatoes relies on visual assessments, which are time-consuming and labour-intensive, with main control measures involving the use of certified tubers, avoiding contamination and removal of affected plants. The timing of detection plays an important role since prompt removal of infected plants minimises the disease spread through the soil, insects and machinery. Early detection, at the very least prior to tuber development, is crucial to minimise chances of cross contamination upon harvest. In this regard, an integrated approach of combining visual assessments with UAV-based sensing to help fine-tune the sensitivity of detection models to the set of symptoms in cultivars at hand would pave a way towards a practical implementation of current approaches, helping reduce labour costs associated with detailed visual inspections and mitigate economic losses caused by blackleg.

5. Conclusions

This study aimed to explore the impact of cultivar and growth stage variations on remote sensing signatures of seed potato plants infected with blackleg disease. By utilising six cultivars with varying susceptibility levels and employing three sensor modalities (hyperspectral, LiDAR, and thermal), we demonstrated that the magnitude of stress responses captured in plant-level metrics varied across modalities and over time. Early-season responses were most strongly reflected in PRI (sensitive to xanthophyll cycle activity), while later in the season, PSRI (sensitive to the carotenoid-to-chlorophyll ratio and senescence) became more informative.

Cultivar-specific traits significantly influenced symptom expression and subsequent remote sensing signatures. Notably, growth stunting and/or dieback were successfully captured in all cultivars for plants infected early in the season, while later in the season, these structural changes were primarily observed in latterly infected plants of cultivars

more prone to dieback. Similarly, thermal metrics, while showing promise, exhibited varying sensitivity to infection across cultivars and growth stages. Importantly, significant variability in thermal signatures was observed even among healthy plants of different cultivars, highlighting the influence of cultivar-specific physiological and morphological characteristics on remote sensing metrics.

While hyperspectral data provided the most valuable information, combining hyperspectral and LiDAR data in SVM detection models yielded the most consistent performance across the investigated dates (balanced accuracy of 90–94 %), showing the added benefit of combining modalities sensitive to different physiological responses. However, differences in growth patterns and symptom expression across cultivars still substantially affected the performance of the investigated SVM detection models. This emphasises the need for better understanding of cultivar-specific responses and the need for further research to address the challenges posed by cultivar variability to ensure the robustness and broad operational applicability of UAV-based remote sensing approaches for disease detection in arable crops.

CRediT authorship contribution statement

Magdalena Smigaj: Writing – review & editing, Writing – original draft, Visualization, Validation, Methodology, Investigation, Formal analysis, Data curation, Conceptualization. **Andries van der Meer:** Writing – review & editing, Validation, Resources, Project administration, Investigation, Data curation. **Jan van der Wolf:** Writing – review & editing, Writing – original draft, Validation, Investigation. **Lammert Kooistra:** Writing – review & editing, Resources, Methodology, Investigation, Conceptualization.

Declaration of competing interest

The authors declare that they have no known competing financial interests or personal relationships that could have appeared to influence the work reported in this paper.

Acknowledgements

This study was undertaken in collaboration with the Wageningen Research Foundation (WR) business unit Field Crops in the framework of the Public-Private Partnership: AGROS use case arable farming. This public Private Partnership was commissioned and funded by TKI Agriculture, Water and Food (project number TKI-LWV: 19143.02).

Supplementary materials

Supplementary material associated with this article can be found, in the online version, at doi:10.1016/j.stress.2025.101120.

Data availability

The authors do not have permission to share data.

References

Avola, G., Di Gennaro, S.F., Cantini, C., Riggi, E., Muratore, F., Tornambè, C., Matese, A., 2019. Remotely sensed vegetation indices to discriminate field-grown olive cultivars. Remote Sens. (Basel) 11 (10), 1242. https://www.mdpi.com/2072-4292/11/10/1242.

Bagy, H.M.M.K., Hassan, E.A., Nafady, N.A., Dawood, M.F.A., 2019. Efficacy of arbuscular mycorrhizal fungi and endophytic strain epicoccum nigrum ASU11 as biocontrol agents against blackleg disease of potato caused by bacterial strain pectobacterium carotovora subsp. Atrosepticum PHY7. Biol. Control 134, 103–113. https://doi.org/10.1016/j.biocontrol.2019.03.005.

Berger, K., Machwitz, M., Kycko, M., Kefauver, S.C., Van Wittenberghe, S., Gerhards, M., Verrelst, J., Atzberger, C., van der Tol, C., Damm, A., Rascher, U., Herrmann, I., Paz, V.S., Fahrner, S., Pieruschka, R., Prikaziuk, E., Buchaillot, M.L., Halabuk, A., Celesti, M., Schlerf, M., 2022. Multi-sensor spectral synergies for crop stress detection and monitoring in the optical domain: a review. Remote Sens. Environ. 280, 113198. https://doi.org/10.1016/j.rse.2022.113198.

Büttner, D., He, S.Y., 2009. Type III protein secretion in plant pathogenic bacteria. Plant Physiol. 150 (4), 1656–1664. https://doi.org/10.1104/pp.109.139089.

Chivasa, W., Mutanga, O., Biradar, C., 2020. UAV-based multispectral phenotyping for disease resistance to accelerate crop improvement under changing climate conditions. Remote Sens (Basel) 12 (15), 2445. https://www.mdpi.com/2072-4292/12/15/2445.

Commission, E., 2020. Farm to fork strategy: for a fair, healthy and environmentally-friendly food system. Commun. Comm. Eur. Parliam. Counc. Eur. Econ. Soc. Comm. Comm. Reg. 381, 1–9.

Cuadros-Casanova, I., Cristiano, A., Biancolini, D., Cimatti, M., Sessa, A.A., Mendez Angarita, V.Y., Dragonetti, C., Pacifici, M., Rondinini, C., Di Marco, M., 2023. Opportunities and challenges for common agricultural policy reform to support the European Green Deal. Conserv. Biol. 37 (3), e14052. https://doi.org/10.1111/cobi.14052.

Eastburn, D.M., McElrone, A.J., Bilgin, D.D., 2011. Influence of atmospheric and climatic change on plant–pathogen interactions. Plant Pathol. 60 (1), 54–69. https://doi.org/10.1111/j.1365-3059.2010.02402.x.

Commission, European, 2019. The european green deal. COM (2019) 640 final. Brussels 11 (12), 2019.

Fallon, B., Yang, A., Lapadat, C., Armour, I., Juzwik, J., Montgomery, R.A., Cavender-Bares, J., 2020. Spectral differentiation of oak wilt from foliar fungal disease and drought is correlated with physiological changes. Tree Physiol. 40 (3), 377–390. https://doi.org/10.1093/treephys/tpaa005.

Franceschini, M.H.D., Brede, B., Kamp, J., Bartholomeus, H., Kooistra, L., 2024. Detection of a vascular wilt disease in potato ('Blackleg') based on UAV hyperspectral imagery: can structural features from LiDAR or SfM improve plant-wise classification accuracy? Comput. Electron. Agric. 227, 109527. https://doi.org/10.1016/j.compag.2024.109527.

Gava, R., Santana, D.C., Cotrim, M.F., Rossi, F.S., Teodoro, L.P.R., da Silva Junior, C.A., Teodoro, P.E., 2022. Soybean cultivars identification using remotely sensed image and machine learning models. Sustainability 14 (12), 7125. https://www.mdpi.com/2071-1050/14/12/7125.

Gold, K.M., Townsend, P.A., Herrmann, I., Gevens, A.J., 2020. Investigating potato late blight physiological differences across potato cultivars with spectroscopy and machine learning. Plant Sci. 295, 110316. https://doi.org/10.1016/j.plantsci.2019.110316.

Guimarães, N., Pádua, L., Sousa, J.J., Bento, A., Couto, P., 2023. Almond cultivar identification using machine learning classifiers applied to UAV-based multispectral data. Int. J. Remote Sens. 44 (5), 1533–1555. https://doi.org/10.1080/01431161.2023.2185913.

Hachoud, S., Sanchez-Muñoz, R., Cusido, R.M., Palazon, J., Zaidi, R.Y., Zaidi, F., 2019. Stimulation of defense reactions in potato against pectobacterium sp. J. Gen. Plant Pathol. 85 (4), 257–272. https://doi.org/10.1007/s10327-019-00843-z.

Hornero, A., Zarco-Tejada, P.J., Marengo, I., Faria, N., Hernández-Clemente, R., 2024. Detection of oak decline using radiative transfer modelling and machine learning from multispectral and thermal RPAS imagery. Int. J. Appl. Earth Obs. Geoinf. 127, 103679. https://doi.org/10.1016/j.jag.2024.103679.

IPPC Secretariat, 2021. Scientific review of the impact of climate change on plant pests – A global challenge to prevent and mitigate plant pest risks in agriculture, forestry and ecosystems. Rome. FAO on behalf of the IPPC Secretariat. doi:10.4060/cb4769en.

Jafar, A., Bibi, N., Naqvi, R.A., Sadeghi-Niaraki, A., Jeong, D., 2024. Revolutionizing agriculture with artificial intelligence: plant disease detection methods, applications, and their limitations [Review]. Front. Plant Sci. 15. https://doi.org/10.3389/fpls.2024.1356260.

Jay, S., Comar, A., Benicio, R., Beauvois, J., Dutartre, D., Daubige, G., Li, W., Labrosse, J., Thomas, S., Henry, N., Weiss, M., Baret, F., 2020. Scoring cercospora leaf spot on sugar beet: comparison of UGV and UAV phenotyping systems. Plant Phenomics 2020. https://doi.org/10.34133/2020/9452123.

Jung, J., Maeda, M., Chang, A., Bhandari, M., Ashapure, A., Landivar-Bowles, J., 2021. The potential of remote sensing and artificial intelligence as tools to improve the resilience of agriculture production systems. Curr. Opin. Biotechnol. 70, 15–22. https://doi.org/10.1016/j.copbio.2020.09.003.

Kariola, T., Brader, G.n., Helenius, E., Li, J., Heino, P., Palva, E.T., 2006. EARLY RESPONSIVE TO DEHYDRATION 15, a negative regulator of abscisic acid responses in Arabidopsis. Plant Physiol. 142 (4), 1559–1573. https://doi.org/10.1104/pp.106.086223.

Kelly, J., Kljun, N., Olsson, P.-O., Mihai, L., Liljeblad, B., Weslien, P., Klemedtsson, L., Eklundh, L., 2019. Challenges and best practices for deriving temperature data from an uncalibrated UAV thermal infrared camera. Remote Sens (Basel) 11 (5), 567.

Kopittke, P.M., Menzies, N.W., Wang, P., McKenna, B.A., Lombi, E., 2019. Soil and the intensification of agriculture for global food security. Environ. Int. 132, 105078. https://doi.org/10.1016/j.envint.2019.105078.

Kovač, M., Ravnikar, M., 1994. The effect of jasmonic acid on the photosynthetic pigments of potato plants grown in vitro. Plant Sci. 103 (1), 11–17. https://doi.org/10.1016/0168-9452(94)03974-7.

Maes, W.H., Steppe, K., 2012. Estimating evapotranspiration and drought stress with ground-based thermal remote sensing in agriculture: a review. J. Exp. Bot. 63 (13), 4671–4712. https://doi.org/10.1093/jxb/ers165.

Maimaitijiang, M., Sagan, V., Sidike, P., Hartling, S., Esposito, F., Fritschi, F.B., 2020. Soybean yield prediction from UAV using multimodal data fusion and deep learning. Remote Sens Environ. 237, 111599. https://doi.org/10.1016/j.rse.2019.111599.

Montesano, M., Scheller, H.V., Wettstein, R., Palva, E.T., 2004. Down-regulation of photosystem I by Erwinia carotovora-derived elicitors correlates with H2O2

accumulation in chloroplasts of potato. Mol. Plant Pathol. 5 (2), 115–123. https://doi.org/10.1111/j.1364-3703.2004.00213.x.

Moshou, D., Pantazi, X.-E., Kateris, D., Gravalos, I., 2014. Water stress detection based on optical multisensor fusion with a least squares support vector machine classifier. Biosyst. Eng. 117, 15–22. https://doi.org/10.1016/j.biosystemseng.2013.07.008.

Mulla, D.J., 2013. Twenty five years of remote sensing in precision agriculture: key advances and remaining knowledge gaps. Biosyst. Eng. 114 (4), 358–371. https://doi.org/10.1016/j.biosystemseng.2012.08.009.

Poblete, T., Navas-Cortes, J.A., Camino, C., Calderon, R., Hornero, A., Gonzalez-Dugo, V., Landa, B.B., Zarco-Tejada, P.J., 2021. Discriminating Xylella fastidiosa from verticillium dahliae infections in olive trees using thermal- and hyperspectral-based plant traits. ISPRS J. Photogramm. Remote Sens. 179, 133–144. https://doi.org/10.1016/j.isprsjprs.2021.07.014.

Poblete, T., Navas-Cortes, J.A., Hornero, A., Camino, C., Calderon, R., Hernandez-Clemente, R., Landa, B.B., Zarco-Tejada, P.J., 2023. Detection of symptoms induced by vascular plant pathogens in tree crops using high-resolution satellite data: modelling and assessment with airborne hyperspectral imagery. Remote Sens. Environ. 295, 113698. https://doi.org/10.1016/j.rse.2023.113698.

Sánchez-Bayo, F., Wyckhuys, K.A.G., 2019. Worldwide decline of the entomofauna: a review of its drivers. Biol. Conserv. 232, 8–27. https://doi.org/10.1016/j.biocon.2019.01.020.

Simões, I.O.P.S., Rios do Amaral, L., 2023. Uav-based multispectral data for sugarcane resistance phenotyping of orange and brown rust. Smart Agric. Technol. 4, 100144. https://doi.org/10.1016/j.atech.2022.100144.

Singh, B.K., Delgado-Baquerizo, M., Egidi, E., Guirado, E., Leach, J.E., Liu, H., Trivedi, P., 2023. Climate change impacts on plant pathogens, food security and paths forward. Nat. Rev. Microbiol. 21 (10), 640–656. https://doi.org/10.1038/s41579-023-00900-7.

Smigaj, M., Agarwal, A., Bartholomeus, H., Decuyper, M., Elsherif, A., de Jonge, A., Kooistra, L., 2024. Thermal infrared remote sensing of stress responses in forest environments: a review of developments, challenges, and opportunities. Curr. For. Rep. 10 (1), 56–76. https://doi.org/10.1007/s40725-023-00207-z.

Smigaj, M., Gaulton, R., Suarez, J.C., Barr, S.L., 2017. Use of miniature thermal cameras for detection of physiological stress in conifers. Remote Sens. (Basel) 9 (9), 957. https://www.mdpi.com/2072-4292/9/9/957.

Smigaj, M., Gaulton, R., Suárez, J.C., Barr, S.L., 2019a. Canopy temperature from an Unmanned aerial Vehicle as an indicator of tree stress associated with red band needle blight severity. For. Ecol. Manage 433, 699–708. https://doi.org/10.1016/j.foreco.2018.11.032.

Smigaj, M., Gaulton, R., Suárez, J.C., Barr, S.L., 2019b. Combined use of spectral and structural characteristics for improved red band needle blight detection in pine plantation stands. For. Ecol. Manage 434, 213–223. https://doi.org/10.1016/j.foreco.2018.12.005.

Steglińska, A., Pielech-Przybylska, K., Janas, R., Grzesik, M., Borowski, S., Kręgiel, D., Gutarowska, B., 2022. Volatile organic compounds and physiological parameters as markers of potato (Solanum tuberosum L.) infection with phytopathogens. Molecules 27 (12), 3708. https://www.mdpi.com/1420-3049/27/12/3708.

Ton, J., Flors, V., Mauch-Mani, B., 2009. The multifaceted role of ABA in disease resistance. Trends Plant Sci. 14 (6), 310–317. https://doi.org/10.1016/j.tplants.2009.03.006.

Toth, I.K., van der Wolf, J.M., Saddler, G., Lojkowska, E., Hélias, V., Pirhonen, M., Tsror, L., Elphinstone, J.G., 2011. Dickeya species: an emerging problem for potato production in Europe. Plant Pathol. 60 (3), 385–399. https://doi.org/10.1111/j.1365-3059.2011.02427.x.

van der Wolf, J.M., De Boer, S.H., 2007. Chapter 27 - bacterial pathogens of potato. In: Vreugdenhil, D., Bradshaw, J., Gebhardt, C., Govers, F., Mackerron, D.K.L., Taylor, M.A., Ross, H.A. (Eds.), Potato Biology and Biotechnology. Elsevier Science B.V, pp. 595–617. https://doi.org/10.1016/B978-044451018-1/50069-5.

van der Wolf, J.M., de Haan, E.G., Kastelein, P., Krijger, M., de Haas, B.H., Velvis, H., Mendes, O., Kooman-Gersmann, M., van der Zouwen, P.S., 2017. Virulence of Pectobacterium carotovorum subsp. Brasiliense on potato compared with that of other pectobacterium and Dickeya species under climatic conditions prevailing in the Netherlands. Plant Pathol 66 (4), 571–583. https://doi.org/10.1111/ppa.12600.

Wan, Q., Brede, B., Smigaj, M., Kooistra, L., 2021. Factors influencing temperature measurements from miniaturized thermal infrared (TIR) cameras: a laboratory-based approach. Sensors 21 (24), 8466. https://www.mdpi.com/1424-8220/21/24/8466.

Weiss, M., Jacob, F., Duveiller, G., 2020. Remote sensing for agricultural applications: a meta-review. Remote Sens. Environ. 236, 111402. https://doi.org/10.1016/j.rse.2019.111402.

Xu, D., Lu, Y., Liang, H., Lu, Z., Yu, L., Liu, Q., 2023. Areca Yellow leaf disease severity monitoring using UAV-based multispectral and thermal infrared imagery. Remote Sens. (Basel) 15 (12), 3114. https://www.mdpi.com/2072-4292/15/12/3114.

Yu, R., Luo, Y., Zhou, Q., Zhang, X., Wu, D., Ren, L., 2021. A machine learning algorithm to detect pine wilt disease using UAV-based hyperspectral imagery and LiDAR data at the tree level. Int. J. Appl. Earth Obs. Geoinf. 101, 102363. https://doi.org/10.1016/j.jag.2021.102363.

Zarco-Tejada, P.J., Camino, C., Beck, P.S.A., Calderon, R., Hornero, A., Hernández-Clemente, R., Kattenborn, T., Montes-Borrego, M., Susca, L., Morelli, M., Gonzalez-Dugo, V., North, P.R.J., Landa, B.B., Boscia, D., Saponari, M., Navas-Cortes, J.A., 2018. Previsual symptoms of Xylella fastidiosa infection revealed in spectral plant-trait alterations. Nat. Plants 4 (7), 432–439. https://doi.org/10.1038/s41477-018-0189-7.

Zarco-Tejada, P.J., Poblete, T., Camino, C., Gonzalez-Dugo, V., Calderon, R., Hornero, A., Hernandez-Clemente, R., Román-Écija, M., Velasco-Amo, M.P., Landa, B.B., Beck, P. S.A., Saponari, M., Boscia, D., Navas-Cortes, J.A., 2021. Divergent abiotic spectral pathways unravel pathogen stress signals across species. Nat. Commun. 12 (1), 6088. https://doi.org/10.1038/s41467-021-26335-3.

Zhang, C., Chen, W., Sankaran, S., 2019. High-throughput field phenotyping of Ascochyta blight disease severity in chickpea. Crop Prot. 125, 104885. https://doi.org/10.1016/j.cropro.2019.104885.

Zhang, N., Chai, X., Li, N., Zhang, J., Sun, T., 2023. Applicability of UAV-based optical imagery and classification algorithms for detecting pine wilt disease at different infection stages. GIsci Remote Sens. 60 (1), 2170479. https://doi.org/10.1080/15481603.2023.2170479.